



Article

# Metallated [3]Ferrocenophanes Containing P<sub>3</sub>M Bridges (M = Li, Na, K) §

Stefan Isenberg, Lisa-Marie Frenzel, Clemens Bruhn and Rudolf Pietschnig \*

Institut für Chemie und CINSaT, Universität Kassel, Heinrich-Plett-Straße 40, 34132 Kassel, Germany; stefan.isenberg@uni-kassel.de (S.I.); lisa-marie@frenzel-owl.de (L.-M.F.); c.bruhn@uni-kassel.de (C.B.)

\* Correspondence: pietschnig@uni-kassel.de; Tel.: +49-561-804-4615

§ Dedicated to Prof. Dr. Dietmar Stalke on the occasion of his 60th birthday.

Received: 19 June 2018; Accepted: 6 July 2018; Published: 11 July 2018



**Abstract:** Alkali-metal phosphanides can be embedded into a [3]ferrocenophane scaffold giving rise to bicyclic ferrocenophanes [MFe(C<sub>5</sub>H<sub>4</sub>P*t*Bu)<sub>2</sub>P] (M = Li, Na, K). Coordination of the alkali-metal ions takes place via the terminal phosphorus atoms adopting a puckered P<sub>3</sub>M four-membered ring. All compounds were characterized via single-crystal X-ray diffraction and multinuclear NMR spectroscopy (<sup>1</sup>H, <sup>31</sup>P, <sup>7</sup>Li), whereas <sup>13</sup>C NMR data could only be recorded for the Li derivative, owing to the limited solubility of its heavier congeners in unreactive solvents.

**Keywords:** alkali metal; phosphorus; ferrocenophane; phosphide; phosphanide

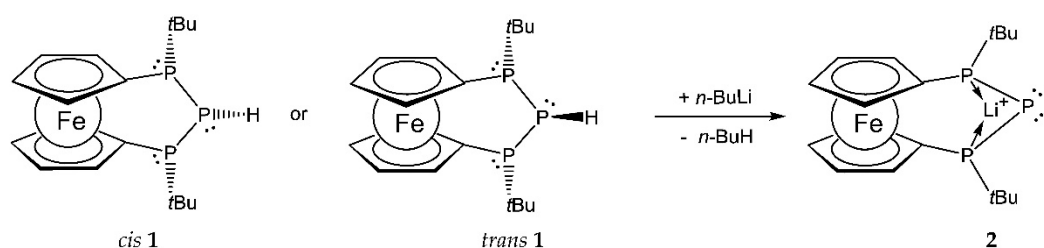
## 1. Introduction

Alkali-metal phosphanides are versatile reagents for connecting phosphorus centers to various functionalities [1,2]. Apart from this role as important synthetic tools, metal phosphanides show a rich structural diversity [1,3]. While metal-rich phosphanides are well known [4], research on saturated phosphorus-rich phosphanides just started emerging [5,6]. In a similar vein, unsaturated phosphorus-rich phosphanides were employed as building blocks for remarkable supramolecular architectures at the limits of molecular chemistry [7–9]. Based on our own efforts in the chemistry of phosphorus-rich ferrocenophanes, we became interested in exploring the metallation of a P–H functionalized bridging unit in a fully phosphorus-bridged [3]ferrocenophane [10–13]. Herein, we report the results of our investigation targeting the metallation of a stereochemically predefined secondary triphosphane constrained by the [3]ferrocenophane scaffold.

## 2. Results and Discussion

Secondary triphosphane (**1**, Scheme 1) was obtained over the course of our investigations dealing with phosphorus-rich ferrocenophanes. It is stereochemically predefined in a way that only the optically inactive *meso* forms, *cis* and *trans* **1**, are obtained, with the terminal bridgehead phosphorus atoms showing opposite absolute configuration, and both *t*-butyl groups pointing to the same side of the molecule [10]. Reaction of a diastereomeric mixture of *cis* and *trans* **1** with *n*-butyl lithium in hexane in the presence of tetramethyl ethylene diamine (TMEDA) afforded the envisaged lithium phosphanide (**2**, Scheme 1) in the form of a single diastereomer (Scheme 1). In the <sup>31</sup>P and <sup>7</sup>Li NMR spectra, **2** was characterized by a characteristic signal splitting (Figure 1). The product showed a <sup>31</sup>P NMR signal at –116.4 ppm (C<sub>6</sub>D<sub>6</sub>) for the central phosphorus atom, split into a triplet owing to coupling with the two chemically equivalent terminal phosphorus atoms (<sup>1</sup>J<sub>PP</sub> = 271 Hz) resonating at 14.9 ppm. In addition to the already mentioned P–P coupling, the doublet of the latter resonance is split into a quartet of equal intensity due to coupling with <sup>7</sup>Li. In line with this, the <sup>7</sup>Li resonance

showed a triplet with  $^1J_{\text{LiP}} = 50$  Hz at 1.4 ppm, indicating symmetric bridging of the two terminal phosphorus atoms via the lithium atom.



**Scheme 1.** Formation of **2** via lithiation of diastereomeric **1**.

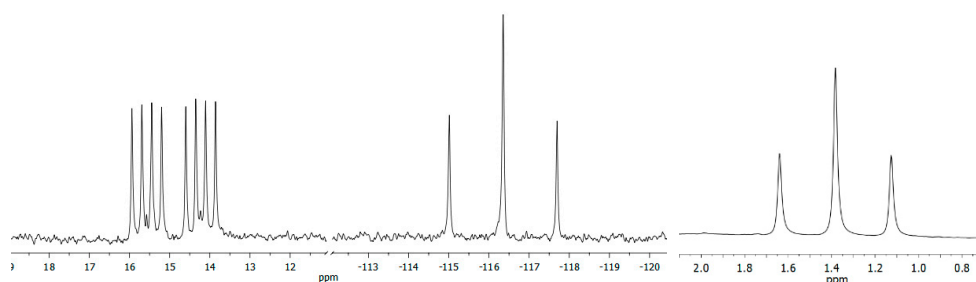


**Figure 1.** Expansion from the  $^{31}\text{P}$  ((left) and (mid), 202 MHz) and  $^7\text{Li}$  ((right), 194 MHz) NMR spectra of **2** (Scheme 1) in benzene- $d_6$  solution at room temperature.

The structural motif of a  $\text{P}_3\text{Li}$  four-membered ring was further corroborated using X-ray diffraction on single-crystalline **2**. It crystallized in a monoclinic space group ( $C2/c$ ) with half a molecule of hexane in the asymmetric unit. The  $\text{P}_3\text{Li}$  unit formed a diamond-like puckered ring, bridging the Cp-rings in this bicyclic [3]ferrocenophane (Figure 2). The lithium atom showed symmetric contacts to the adjacent phosphorus atoms (2.662(3) Å and 2.548(3) Å), and a distance of 3.455(3) Å to the formal phosphanide center. The P–Li distances in **2** were close to those observed in anionic 1,3-diphospha-2-silaallylic systems with lithium as a counter ion [14]. The P–P bond lengths in **2**, between the central phosphorus and the adjacent terminal phosphorus atoms, were 2.1710(8) Å and 2.1670(8) Å. This triphospha metallacycle folded with an angle of 135.89(6)° (Figure 2). The coordination sphere of lithium was completed by one molecule of TMEDA. The respective Li–N distances were placed with 2.113(4) Å and 2.080(4) Å in the expected range known from comparable compounds [15,16]. Owing to steric effects, the coordination geometry around lithium differed from an ideal tetrahedron with angles of 119.8(1)° to 135.6(2)°, showing larger values toward the ferrocene backbone. The Cp rings of the ferrocene unit showed a nearly eclipsed conformation (torsion angle of about 2°), and opened an interplanar angle of 3.3(1)° toward the lithium TMEDA adduct.

The structural situation is closely related to the dilithiated bisphosphanide  $[\text{Fe}(\text{Cp}-\text{P}(\text{Li})t\text{Bu})_2]$ , where two phosphorus atoms are symmetrically bridged by two lithium atoms forming a  $\text{P}_2\text{Li}_2$  four-membered ring in the solid state and in solution [11,15]. Similarly, the spectroscopic data are comparable to the latter bisphosphanide, as well as to other dimeric lithium phosphanides [5,17]. Phosphanide **2** was very sensitive to air and moisture, and was stable only in hydrocarbon solvents.

In order to explore the accessibility of the sodium analog of **2**, we reacted **1** with sodium hydride in the presence of [15]-crown-5 in tetrahydrofuran (THF) solution. The solution turned light-red over a period of 12 h, indicating the formation of sodium phosphanide (**3**, Scheme 2). The mixture was stirred for an additional 24 h for completion. In the  $^{31}\text{P}$  NMR spectra, **3** was characterized by a resonance at  $-100.3$  ppm (THF- $d_8$ ) for the central phosphorus atom, which splits into a pseudo triplet with a pseudo coupling constant of  $^1J_{\text{PP}} = 277$  Hz. The two chemically equivalent terminal phosphorus atoms showed a single doublet at 21.3 ppm, with a matching coupling constant to the central phosphorus atom.

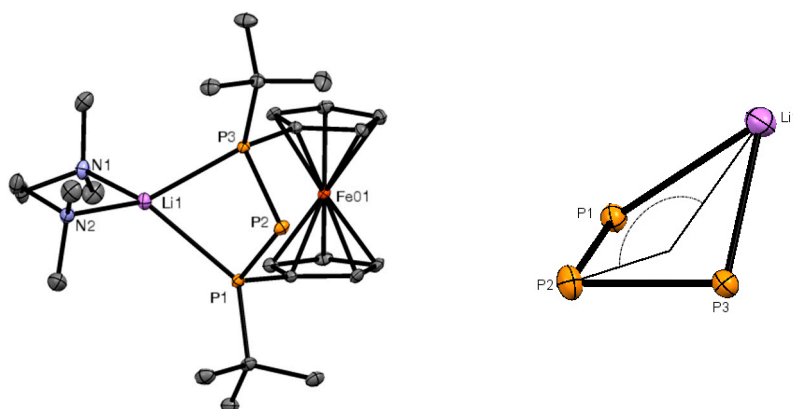
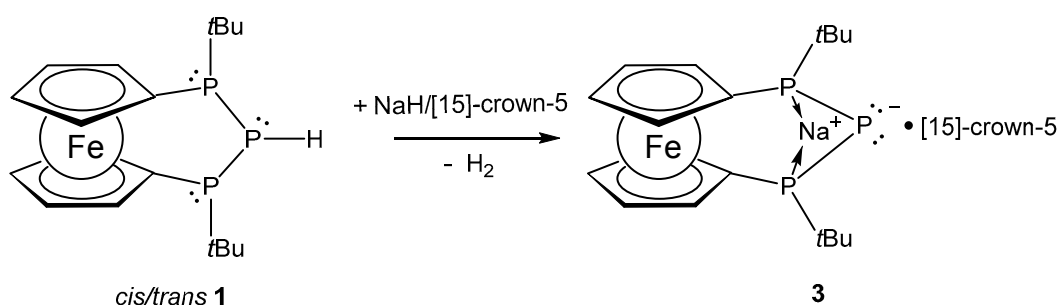


**Figure 2.** ORTEP plot of the molecular structure of **2** (left), and expansion of the folded P<sub>3</sub>Li ring (right). Ellipsoids were drawn at the 30% probability level. Hydrogen atoms were omitted for clarity.



**Scheme 2.** Formation of **3** via deprotonation of **1**.

Again, single crystals suitable for X-ray diffraction could be obtained, confirming the presence of the P<sub>3</sub>Na motif also in this heavier alkali phosphanide (Figure 3). Compound **3** crystallized in a monoclinic space group (P2<sub>1</sub>/c), with a somewhat smaller interplanar angle (3.1(1)°) compared to **2**, and a bigger torsion angle of the ferrocene backbone (about 3°). Similar to **2**, the P<sub>3</sub>Na unit formed a diamond-like puckered ring which was more folded (129.63(3)°) than in its lithium congener. The sodium atom showed symmetric contacts to the adjacent phosphorus atoms (3.037(2) Å and 3.107(2) Å), and a distance of 3.868(1) Å to the formal phosphanide center. The P–P bond lengths between the latter and the adjacent phosphorus atoms were 2.184(2) Å and 2.174(2) Å. The coordination sphere of sodium was completed by one molecule of [15]-crown-5. The respective Na–O distances lay in the range of 2.453(2) Å to 2.607(2) Å, with an average distance of 2.498(2) Å, which matched values known in literature [18–23]. In contrast to the number of published potassium triphosphanides, characterized sodium triphosphanides are scarce. Nevertheless, the available <sup>31</sup>P chemical shifts in the literature fit our results quite well [24]. Furthermore, Grützmaier et al. described a P<sub>3</sub> phosphanediide ion with similar bond distances between the sodium cation and the phosphanide centers, as well as similar described phosphorus–phosphorus distances [25]. Even the Na–P distances in triphosphaallylic sodium were close to those found in **3**, despite the quite different bonding situation of the π-conjugated species [26].

To amend this series of closely related alkali-metal triphosphanides, we set out to prepare the corresponding potassium compound, **4** (Scheme 3). While the deprotonation of **1** with potassium hydride was precluded by the intrinsically low solubility of this reagent, we were able to achieve deprotonation using potassium *t*-butoxide (KO*t*Bu). Owing to the limited solubility of KO*t*Bu in neat hydrocarbons, the reaction had to be carried out in coordinating solvents such as THF (Scheme 3). The formation of **4** was indicated by an instantaneous color change showing a deep-red solution. In the <sup>31</sup>P NMR spectra, **4** was characterized by a resonance of the central phosphanide atom as a triplet

at  $-107.3$  ppm (THF- $d_8$ ) with a  $^1J_{PP}$  coupling of 268 Hz. The corresponding doublet was located at 16.8 ppm.

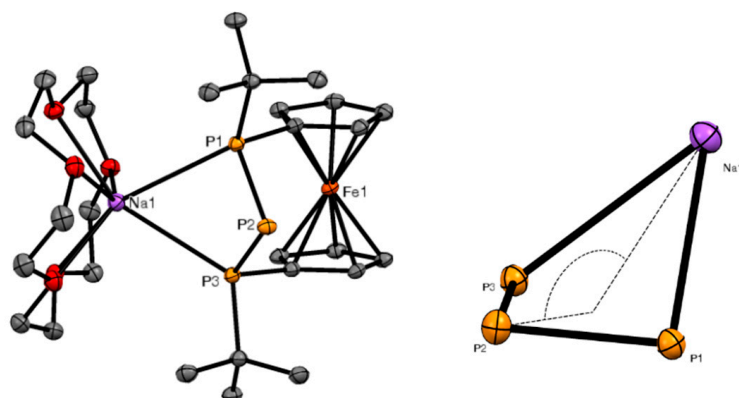
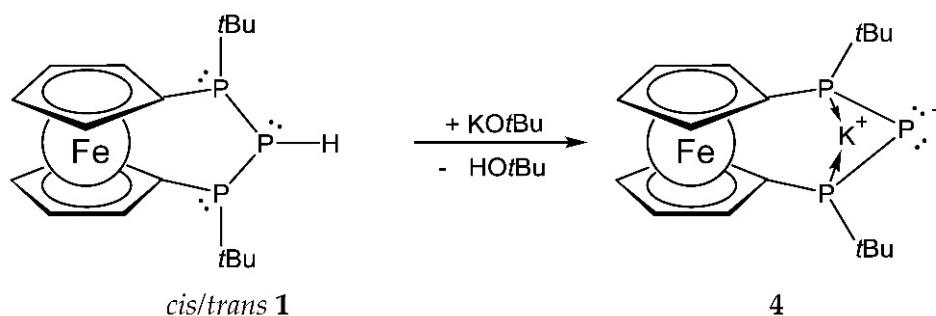


**Figure 3.** ORTEP plot of the molecular structure of **3** (Scheme 2; (left)) and expansion of the folded P<sub>3</sub>Na ring (right). Ellipsoids were drawn at the 30% probability level. Hydrogen atoms were omitted for clarity.



**Scheme 3.** Formation of **4** via direct metallation of **1**.

Microcrystalline and poorly soluble **4** was recrystallized in the presence of [18]-crown-6 affording single-crystalline samples suitable for X-ray diffraction. The heaviest alkali metal of our series showed a similar P<sub>3</sub>K motif to that in its lighter analogs (Figure 4). Compound **4**·[18]-crown-6 crystallized in a triclinic space group ( $P\bar{1}$ ), and showed a less strained (interplanar angle  $2.1(5)^\circ$ ) but more staggered (torsion angle about  $5^\circ$ ) structure. Similar to **2** and **3**, the P<sub>3</sub>K unit formed a diamond-like puckered ring which was more folded ( $125.5(1)^\circ$ ) than in the Li/Na congeners, possibly caused by the introduction of a sterically more demanding crown ether. The potassium atom showed slight asymmetric contacts to the adjacent phosphorus atoms ( $3.581(3)$  Å and  $3.333(2)$  Å), and a distance of  $4.227(3)$  Å to the formal phosphanide center. The P–P bond lengths between the latter and the adjacent phosphorus atoms were  $2.187(2)$  Å and  $2.192(4)$  Å, and the folding angle of the puckered ring was smallest in this series. The coordination sphere of potassium was completed by one molecule of [18]-crown-6, adding up to a total coordination number of eight around the potassium atom. The respective K–O distances lay in the range of  $2.748(8)$  Å to  $3.039(8)$  Å, showing an average distance of  $2.88(1)$  Å. This was in line with similar distances in the literature [18,19,27,28]. The crown ether showed disorder at the carbon and oxygen atoms, in which ellipsoids stretched along the ring, indicating different positions of the crown in the crystal by rotation about the potassium center. This disorder limited the R value to 0.1104.

As already mentioned, phosphanides **2–4** were extremely sensitive to air and moisture, and traces of residual water or reactive solvents available for deprotonation, such as THF, led to protonation of **2–4**, resulting in the formation of **1**, which precluded the isolation of **2–4** in an analytically pure form. Interestingly, the protonation of isostructural phosphanides **2–4** resulted exclusively in the formation of *trans* **1**. We assume that this selectivity most likely originated from the preferential attack of water

from the metal side for kinetic reasons, since the energy difference between *cis* and *trans* **1** was only small in favor of the *trans* isomer (0.1 kcal/mol at the B3LYP/6-311+G\*\* level of theory) [10].

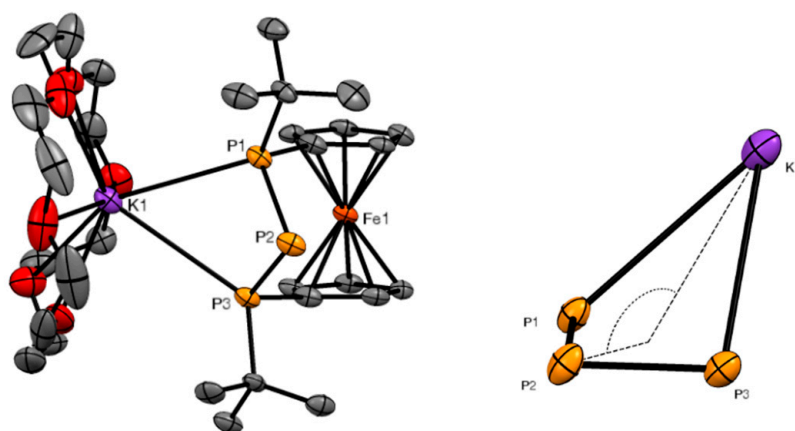


**Figure 4.** ORTEP plot of 4-[18]-crown-6 (Scheme 3; (left)) and expansion of the folded P<sub>3</sub>K ring (right). Ellipsoids were drawn at the 30% probability level. Hydrogen atoms were omitted for clarity.

The heteronuclear NMR data did not follow a clear trend along the series of alkali-metal cations from Li<sup>+</sup> to K<sup>+</sup> in line with observations reported in the literature [24]. Compared with the parent hydrophosphane, **1**, the formal phosphanide centers in deprotonated **2–4** were more shielded with respect to *cis* **1**, but deshielded with respect to *trans* **1**. The adjacent phosphorus atoms were shifted downfield upon interaction with the alkali-metal cations ( $\delta(^{31}\text{P})$ : *cis* **1**:  $-74.3/-9.8$  ppm; *trans* **1**:  $-125.1/-6.5$  ppm [10]; **2**:  $-116.4/14.9$  ppm; **3**:  $-100.3/21.3$  ppm; **4**:  $-107.3/16.8$  ppm). The  $^1J_{\text{PP}}$  coupling constants of **2–4** were quite similar (**2**: 271 Hz; **3**: 277 Hz; **4**: 268 Hz), with values between those observed for *cis* and *trans* **1** (*cis*: 295/289 Hz; *trans*: 107 Hz), indicating reduced P–P interaction compared to the *cis* isomer **1**, in which the lone pairs of all phosphorus atoms were located on the same side of the molecule [10]. In turn, the additional electron pair at the formal phosphanide center in **2–4** increased the interaction compared with *trans* **1** [29,30].

With increasing size of the alkali metal, the diamond-shaped ring was more folded, possibly owing to repulsive interactions between the crown ether and the ferrocene backbone. As a consequence of this steric effect, the torsion angle of the ferrocene unit slightly increased within the series, whereas the interplanar angle of the Cp rings decreased. Similar structural effects could be observed in triphospha[3]ferrocenophanes substituted with sterically demanding alkyl groups [10]. The M–P2 distances in **2–4** were all slightly below the sum of the Van-der-Waals radii [31]. However, the interaction between the alkali metal and P2 was most likely electrostatic in nature. The distances of the formal phosphanide atom to the iron center of the ferrocene backbone were almost identical for **2–4** (ca. 3.9 Å), and matched the value for the parent phosphane, **1**, to which they were isostructural [10].

### 3. Experimental Details

All manipulations were carried out under inert argon atmosphere using a standard Schlenk technique. All solvents were dried and freshly distilled over an Na/K-alloy where applicable. Compound **1** was prepared according to a previously published procedure [10]. All other reagents were purchased and used without further purification.  $^1\text{H}$ ,  $^{13}\text{C}$ , and  $^{31}\text{P}$  NMR spectra were recorded on a Varian VNMR5-500 MHz spectrometer (Varian Inc., Palo Alto, CA, USA) at room temperature using tetramethylsilane (TMS) as the external reference for  $^1\text{H}$  and  $^{13}\text{C}$  nuclei.  $^{13}\text{C}$ – $^1\text{H}$  correlation was used for the detailed chemical shift assignments in **2**. For multiplets, chemical shifts were reported as the center of the respective multiplet.

### 3.1. Synthesis of Compound 2

To a stirred mixture of 0.16 g (0.4 mmol) of **1** and 0.1 mL (0.7 mmol) of TMEDA in 5 mL hexane, 0.16 mL (0.4 mmol; 2.5 M) of *n*BuLi in hexane was added dropwise at room temperature. After 2 h, the resulting orange precipitate was filtered off and washed with 1 mL of pentane. The product was obtained as an orange solid. Single crystals suitable for X-ray diffraction analysis could be obtained via recrystallization from hexane. Yield: 0.18 g (89%).  $^1\text{H}$  NMR (500 MHz,  $\text{C}_6\text{D}_6$ ):  $\delta$  = 1.52 (m, 18H, *t*Bu), 1.68 (*br s*, 4H,  $\text{CH}_2$ ), 2.01 (*br s*, 12H,  $\text{N}(\text{CH}_3)_2$ ), 4.04 (m, 2H, Cp), 4.28 (m, 2H, Cp), 4.35 (m, 2H, Cp), 5.15 (m, 2H, Cp) ppm;  $^{13}\text{C}\{^1\text{H}\}$  NMR (126 MHz,  $\text{C}_6\text{D}_6$ ):  $\delta$  = 31.1 (m, *t*Bu  $\text{C}_q$ ), 31.3 (m, *t*Bu  $\text{CH}_3$ ), 46.5 (s,  $\text{N}(\text{CH}_3)_2$ ), 56.6 (s,  $\text{CH}_2$ ), 67.6 (m, Cp), 71.0 (s, Cp), 72.3 (m, Cp), 77.0 (m, Cp), 91.5 (m, Cp  $\text{C}_{\text{ipso}}$ ) ppm;  $^{31}\text{P}$  NMR (202 MHz,  $\text{C}_6\text{D}_6$ ):  $\delta$  =  $-116.4$  (t, 1P,  $^1J_{\text{PP}} = 271$  Hz,  $\text{P}^-$ ), 14.9 (dq, 2P,  $^1J_{\text{PP}} = 271$  Hz,  $^1J_{\text{PLi}} = 50$  Hz, P *t*Bu).  $^7\text{Li}$  NMR (194 MHz,  $\text{C}_6\text{D}_6$ ):  $\delta$  = 1.4 (t,  $^1J_{\text{LiP}} = 50$  Hz).

### 3.2. Synthesis of Compound 3

Firstly, 0.078 g (0.2 mmol) of **1**, 0.005 g (0.2 mmol) of sodium hydride, and 0.022 g (0.2 mmol) of 15-crown-5 were dissolved in THF (2 mL), and stirred for two days at room temperature. A red solid precipitated from the former orange solution, which was separated by filtration. The remaining solid was washed with pentane ( $2 \times 5$  mL), and gave **3** as a light-red solid. Recrystallization from THF afforded single crystals suitable for X-ray diffraction analysis. Yield: 0.10 g (78%).  $^1\text{H}$  NMR (500 MHz, THF- $d_8$ ):  $\delta$  = 1.17 (m, 18H, *t*Bu), 3.59 (m, 20H, 15-crown-5), 3.76 (m, 2H, Cp), 4.07 (m, 2H, Cp), 4.29 (m, 2H, Cp), 4.66 (m, 2H, Cp) ppm;  $^{31}\text{P}$  NMR (202 MHz, THF- $d_8$ ):  $\delta$  =  $-100.3$  (pseudo t, 1P,  $^1J_{\text{PP}} = 277$  Hz,  $\text{P}^-$ ), 21.3 (d, 1P,  $^1J_{\text{PP}} = 277$  Hz, P *t*Bu).

### 3.3. Synthesis of Compound 4

To a stirred dry mixture of 0.118 g (0.3 mmol) of **1** and 0.034 g (0.3 mmol) of KO*t*Bu, 3 mL of THF was added at room temperature. The solution immediately turned deep red, and stirring was continued for an additional 30 min. All volatiles were removed under reduced pressure, and the residue was kept under vacuum for at least 1 h. Then, 2 mL of THF and 0.080 g (0.3 mmol) of 18-crown-6 were added to the residue, and stirred for 5 min. After removing the solvent in vacuo, the product was obtained as a red solid. Recrystallization from THF afforded crystals suitable for X-ray diffraction analysis. Yield: 0.14 g (65%).  $^1\text{H}$  NMR (500 MHz, THF- $d_8$ ):  $\delta$  = 1.13 (m, 18H, *t*Bu), 3.14–3.50 (*br s*, 24H, 18-crown-6), 3.80 (m, 2H, Cp), 4.09 (m, 2H, Cp), 4.13 (m, 2H, Cp), 4.64 (m, 2H, Cp) ppm;  $^{31}\text{P}$  NMR (202 MHz, THF- $d_8$ ):  $\delta$  =  $-107.3$  (t, 1P,  $^1J_{\text{PP}} = 268$  Hz,  $\text{P}^-$ ), 16.8 (d, 2P,  $^1J_{\text{PP}} = 268$  Hz, P *t*Bu).

### 3.4. X-ray Crystallography

X-ray diffraction measurements were performed on a Stoe IPDS 2 diffractometer (**3**) (STOE & Cie. GmbH, Darmstadt, Germany) with an image plate detector and monochromated (graded multilayer mirror) Mo  $\text{K}\alpha$  radiation (Mo Genix), or on a Stoe StadiVari diffractometer (**2** and **4**) with a Dectris Pilatus 200 K detector using monochromated (graded multilayer) Cu  $\text{K}\alpha$  radiation (Cu Genix) (Xenocs, Sassenage, France). The datasets were recorded with  $\omega$ -scans, and corrected for Lorentz, polarization, and absorption effects. The structures were solved using direct methods and refined without restraints by full-matrix least-squares techniques against  $F^2$  (SHELXT and SHELXL-2014/7) [32]. Details of the structure determinations and refinement for **2–4** are summarized in Table 1. Further programs used for analysis and visualization of structural information included WinGX and Mercury [33,34]. CCDC 1847287–1847289 contains the supplementary crystallographic data for this paper (See Supplementary Materials). These data are provided free of charge by the Cambridge Crystallographic Data Centre.

**Table 1.** Crystal data and structure refinement for Compounds 2–4 (Schemes 1–3).

	2	3	4
Formula	C <sub>24</sub> H <sub>42</sub> FeLiN <sub>2</sub> P <sub>3</sub> ·0.5(C <sub>6</sub> H <sub>14</sub> )	C <sub>28</sub> H <sub>46</sub> FeNaO <sub>5</sub> P <sub>3</sub>	C <sub>30</sub> H <sub>50</sub> FeKO <sub>6</sub> P <sub>3</sub>
Formular weight	557.38	634.40	694.56
Temperature (K)	100	100	100
Wavelength (Å)	1.54186	0.71073	1.54186
Crystal system	monoclinic	monoclinic	triclinic
Space group	C2/c	P2 <sub>1</sub> /c	P-1
Unit-cell dimensions:			
<i>a</i> (Å)	10.2172(3)	14.2758(6)	10.791(1)
<i>b</i> (Å)	17.3386(6)	10.3266(3)	10.7753(10)
<i>c</i> (Å)	34.6955(9)	21.4828(9)	16.8369(16)
α (°)	90	90	73.904(7)
β (°)	90.735(2)	99.536(3)	71.663(7)
γ (°)	90	90	69.620(7)
Volume (Å <sup>3</sup> )	6145.9(3)	3123.2(2)	1710.8(3)
Z	8	4	2
Calculated density (mg/m <sup>3</sup> )	1.205	1.349	1.348
μ (mm <sup>-1</sup> )	5.526	0.685	6.265
Θ-range for data collected (°)	5.100–68.990	1.446–25.498	2.815–68.998
Data/parameters	5340/318	5814/349	6198/376
Goodness-of-fit on F <sup>2</sup>	1.021	1.047	1.024
R <sub>1</sub> (observed data)	0.0309	0.0531	0.1104
wR <sub>2</sub> (all data)	0.0733	0.1559	0.3201
R <sub>int</sub>	0.0240	0.0654	0.0772
r.e.d. min/max (e·Å <sup>-3</sup> )	0.539/0.834	−0.944/0.776	0.451/0.887

#### 4. Conclusions

In summary, we demonstrated that secondary triphosphanides of the alkali metals, M = Li, Na, K, could be embedded into a [3]ferrocenophane scaffold, giving rise to bicyclic ferrocenophanes with a two-fold intramolecular P→M donor stabilization as part of puckered P<sub>3</sub>M rings. The folding of these rings became more pronounced as the alkali-metal cation increased in size. Compounds 3 and 4 were limited in solubility to organic polar solvents, such as THF, while 2 was soluble in nonpolar solvents as well. All alkali-metal cations required coordination of additional donors to complete their coordination spheres. Nevertheless, all compounds were highly sensitive to air and moisture in solution and in the solid state. It is worth noting that the formally hydridic P–H bond (according to a difference in electronegativity) clearly behaved in a protic nature with all reagents under investigation, even though secondary triphosphane lacked any electronegative substituents at phosphorus. Remarkably, the protonation of phosphanides 2–4 led to the stereoselective formation of *trans* 1, which was otherwise not accessible.

**Supplementary Materials:** The following are available online at <http://www.mdpi.com/2304-6740/6/3/67/s1>. Cif and checkcif files of complexes 2–4.

**Author Contributions:** I.S. and L.-M.F. performed the experiments, and analyzed the spectroscopic data; C.B. performed the X-ray interpretation; R.P. provided the materials and wrote the paper.

**Funding:** German Science fund (DFG, PI 353/8-1 and CRC 1319).

**Acknowledgments:** The authors would like to thank the German Science fund (DFG, PI 353/8-1 and CRC 1319) for financial support.

**Conflicts of Interest:** The authors declare no conflict of interest.

## References

1. Izod, K. Group I complexes of P- and as-donor ligands. *Adv. Inorg. Chem.* **2000**, *50*, 33–107.
2. Fritz, G.; Scheer, P. Silylphosphanes: Developments in Phosphorus Chemistry. *Chem. Rev.* **2000**, *100*, 3341–3402. [[CrossRef](#)] [[PubMed](#)]
3. Rosenberg, L. Metal complexes of planar PR<sub>2</sub> ligands: Examining the carbene analogy. *Coord. Chem. Rev.* **2012**, *256*, 606–626. [[CrossRef](#)]
4. Driess, M.; Nöth, H. *Molecular Clusters of the Main Group Elements*; Wiley-VCH: Weinheim, Germany, 2004.
5. Wolf, R.; Schisler, A.; Lönnecke, P.; Jones, C.; Hey-Hawkins, E. Syntheses and Molecular Structures of Novel Alkali Metal Tetraorganylcyclopentaphosphanides and Tetraorganyltetraphosphane-1, 4-diides. *Eur. J. Inorg. Chem.* **2004**, *16*, 3277–3286. [[CrossRef](#)]
6. Wolf, R.; Gomez-Ruiz, S.; Reinhold, J.; Boehlmann, W.; Hey-Hawkins, E. The (P<sub>4</sub>HMes<sub>4</sub>)<sup>−</sup> anion: Lability, fluxionality, and structural ambiguity (Mes = 2,4,6-Me<sub>3</sub>C<sub>6</sub>H<sub>2</sub>). *Inorg. Chem.* **2006**, *45*, 9107–9113. [[CrossRef](#)] [[PubMed](#)]
7. Dielmann, F.; Heindl, C.; Hastreiter, F.; Peresyphkina, E.V.; Virovets, A.V.; Gschwind, R.M.; Scheer, M. A nano-sized Supramolecule beyond the Fullerene Topology. *Angew. Chem. Int. Ed.* **2014**, *53*, 13605–13608. [[CrossRef](#)] [[PubMed](#)]
8. Scheer, M.; Schindler, A.; Merkle, R.; Johnson, B.P.; Linseis, M.; Winter, R.; Anson, C.E.; Virovets, A.V. Fullerene C<sub>60</sub> as an Endohedral Molecule within an Inorganic Supramolecule. *J. Am. Chem. Soc.* **2007**, *129*, 13386–13387. [[CrossRef](#)] [[PubMed](#)]
9. Bai, J.; Virovets, A.V.; Scheer, M. Synthesis of Inorganic Fullerene-Like Molecules. *Science* **2003**, *300*, 781–783. [[CrossRef](#)] [[PubMed](#)]
10. Borucki, S.; Kelemen, Z.; Maurer, M.; Bruhn, C.; Nyulászi, L.; Pietschnig, R. Stereochemical alignment in triphospha-[3]ferrocenophanes. *Chem. Eur. J.* **2017**, *23*, 10438–10450. [[CrossRef](#)] [[PubMed](#)]
11. Kargin, D.; Kelemen, Z.; Krekić, K.; Maurer, M.; Bruhn, C.; Nyulászi, L.; Pietschnig, R. [3]Ferrocenophanes with bisphosphanotetryl bridge: Inorganic rings on the way to tetrylenes. *Dalton Trans.* **2016**, *45*, 2180–2189. [[CrossRef](#)] [[PubMed](#)]
12. Moser, C.; Belaj, F.; Pietschnig, R. Phosphorus-Rich Ferrocenophanes. *Phosphorus Sulfur Silicon Relat. Elem.* **2015**, *190*, 837–844. [[CrossRef](#)]
13. Moser, C.; Belaj, F.; Pietschnig, R. Diphospha[2]ferrocenophane alias (1,4-dihydrotetraphosphaneoxide): Stereoselective formation via hydrolytic P-P bond formation. *Chem. Eur. J.* **2009**, *15*, 12589–12591. [[CrossRef](#)] [[PubMed](#)]
14. Lange, D.; Klein, E.; Bender, H.; Niecke, E.; Nieger, M.; Pietschnig, R.; Schoeller, W.W.; Ranaivonjatovo, H. 1,3-Diphospha-2-silaallylic Lithium Complexes and Anions: Synthesis, Crystal Structures, Reactivity, and Bonding Properties. *Organometallics* **1998**, *17*, 2425–2432. [[CrossRef](#)]
15. Hitzel, S.; Färber, C.; Bruhn, C.; Siemeling, U. Phosphido complexes derived from 1,1'-ferrocenediyl-bridged secondary diphosphines. *Dalton Trans.* **2017**, *46*, 6333–6348. [[CrossRef](#)] [[PubMed](#)]
16. Less, R.J.; Naseri, V.; Wright, D.S. Formation of an organometallic phosphanediide via main-group dehydrocoupling. *Organometallics* **2009**, *28*, 1995–1997. [[CrossRef](#)]
17. Reich, H.J.; Dykstra, R.R. Solution Structure of Lithium Benzeneselenolate and Lithium Diphenylphosphide: NMR Identification of Cyclic Dimers and Mixed Dimers. *Organometallics* **1994**, *13*, 4578–4585. [[CrossRef](#)]
18. Poonia, N.S.; Bajaj, A.V. Coordination chemistry of alkali and alkaline earth cations. *Chem. Rev.* **1979**, *79*, 389–445. [[CrossRef](#)]
19. Bajaj, A.V.; Poonia, N.S. Comprehensive coordination chemistry of alkali and alkaline earth cations with macrocyclic multidentates: Latest position. *Coord. Chem. Rev.* **1988**, *87*, 55–213. [[CrossRef](#)]
20. Berry, A.; Green, M.L.H.; Bandy, J.A.; Prout, K. Transition Metal-Hydrogen-Alkali Metal Bonds: Synthesis and Crystal Structures of [K(18-crown-6)][W(PMe<sub>3</sub>)<sub>3</sub>H<sub>5</sub>], [Na(15-crown-5)][W(PMe<sub>3</sub>)<sub>3</sub>H<sub>5</sub>] and [(W(PMe<sub>3</sub>)<sub>3</sub>H<sub>5</sub>Li)<sub>4</sub>] and Related Studies. *J. Chem. Soc. Dalton Trans.* **1991**, 2185–2206. [[CrossRef](#)]
21. Gjikaj, M.; Adam, A. Complexation of Alkali Triflates by Crown Ethers: Synthesis and Crystal Structure of [Na(12-crown-4)<sub>2</sub>][SO<sub>3</sub>CF<sub>3</sub>], [Na(15-crown-5)][SO<sub>3</sub>CF<sub>3</sub>], [Rb(18-crown-6)][SO<sub>3</sub>CF<sub>3</sub>], and [Cs(18-crown-6)][SO<sub>3</sub>CF<sub>3</sub>]. *Z. Anorg. Allg. Chem.* **2006**, *632*, 2475–2480. [[CrossRef](#)]
22. Nöth, H.; Warchhold, M. Sodium Hydro(isothiocyanato)borates: Synthesis and Structures. *Eur. J. Inorg. Chem.* **2004**, *2004*, 1115–1124. [[CrossRef](#)]

23. Cole, M.L.; Jones, C.; Junk, P.C. Ether and crown ether adduct complexes of sodium and potassium cyclopentadienide and methylcyclopentadienide—Molecular structures of  $[\text{Na}(\text{dme})\text{Cp}]_{\infty}$ ,  $[\text{K}(\text{dme})_{0.5}\text{Cp}]_{\infty}$ ,  $[\text{Na}(\text{15-crown-5})\text{Cp}]$ ,  $[\text{Na}(\text{18-crown-6})\text{Cp}^{\text{Me}}]$  and the “naked Cp<sup>-</sup>” complex  $[\text{K}(\text{15-crown-5})_2][\text{Cp}]$ . *J. Chem. Soc. Dalton Trans.* **2002**, 896–905. [[CrossRef](#)]
24. Schmidpeter, A.; Burget, G. Die Reaktion Von Alkaliphosphiden Mit Weisssem Phosphor, 1<sup>1</sup> Bildung Von 1,1,3,3-Tetraphenyl-Triphosphid, 2,3,4,5-Tetraphenyl-Cyclopentaphosphid und Phenyl-Tricycloheptaphosphid. *Phosphorus Sulfur Silicon Relat. Elem.* **1985**, *22*, 323–335. [[CrossRef](#)]
25. Geier, J.; Ruegger, H.; Worle, M.; Grützmacher, H. Sodium oligophosphanediide ions in the  $\text{PhPCl}_2/\text{Na}$  system: Syntheses and structural characterization. *Angew. Chem. Int. Ed.* **2003**, *42*, 3951–3954. [[CrossRef](#)] [[PubMed](#)]
26. Wiberg, N.; Wörner, A.; Lerner, H.W.; Karaghiosoff, K.; Fenske, D.; Baum, G.; Dransfeld, A.; von Ragué Schleyer, P. The Triphosphide  $(\text{tBu}_3\text{Si})_2\text{P}_3\text{Na}$ : Formation, X-ray and Ab initio Structure Analyses, Protonation and Oxidation to Triphosphane  $(\text{tBu}_3\text{Si})_2\text{P}_3\text{H}$  and Hexaphosphanes  $(\text{tBu}_3\text{Si})_4\text{P}_6$ . *Eur. J. Inorg. Chem.* **1998**, *1998*, 833–841. [[CrossRef](#)]
27. Thiele, G.; Vondung, L.; Donsbach, C.; Pulz, S.; Dehnen, S. Organic Cation and Complex Cation-Stabilized (Poly-)Selenides,  $[\text{Cation}]_x(\text{Se}_y)_z$ : Diversity in Structures and Properties. *Z. Anorg. Allg. Chem.* **2014**, *640*, 2684–2700. [[CrossRef](#)]
28. Kobrsi, I.; Zheng, W.; Knox, J.E.; Heeg, M.J.; Schlegel, H.B.; Winter, C.H. Experimental and theoretical study of the coordination of 1, 2, 4-triazolato, tetrazolato, and pentazolato ligands to the  $[\text{K}(\text{18-crown-6})]^+$  fragment. *Inorg. Chem.* **2006**, *45*, 8700–8710. [[CrossRef](#)] [[PubMed](#)]
29. Hahn, J. Higher order <sup>31</sup>P NMR Spectra of Polyphosphorus Compounds. In *Phosphorus-31 NMR Spectroscopy in Stereochemical Analysis*; Verkade, J.G., Quin, L.D., Eds.; VCH: Weinheim, Germany, 1987; pp. 331–364.
30. Albrand, J.P.; Faucher, H.; Gagnaire, D.; Robert, J.B. Calculation of the <sup>1</sup>J<sub>(PP)</sub> angular dependence in P<sub>2</sub>H<sub>4</sub>. *Chem. Phys. Lett.* **1976**, *38*, 521–523. [[CrossRef](#)]
31. Bondi, A. van der Waals volumes and radii. *J. Phys. Chem.* **1964**, *68*, 441–451. [[CrossRef](#)]
32. Sheldrick, G.M. A short history of SHELX. *Acta Crystallogr. A* **2008**, *64*, 112–122. [[CrossRef](#)] [[PubMed](#)]
33. Farrugia, L.J. WinGX suite for small-molecule single-crystal crystallography. *J. Appl. Crystallogr.* **1999**, *32*, 837–838. [[CrossRef](#)]
34. Macrae, C.F.; Edgington, P.R.; McCabe, P.; Pidcock, E.; Shields, G.P.; Taylor, R.; Towler, M.; van der Streek, J. Mercury: Visualization and analysis of crystal structures. *J. Appl. Crystallogr.* **2006**, *39*, 453–457. [[CrossRef](#)]



© 2018 by the authors. Licensee MDPI, Basel, Switzerland. This article is an open access article distributed under the terms and conditions of the Creative Commons Attribution (CC BY) license (<http://creativecommons.org/licenses/by/4.0/>).